JOURNAL OF AGRICULTURAL AND FOOD CHEMISTRY

Article

pubs.acs.org/JAFC

Abiotic Degradation of Glyphosate into Aminomethylphosphonic Acid in the Presence of Metals

J. Ascolani Yael,[†] J. D. Fuhr,[†,‡] G. A. Bocan,[‡] A. Daza Millone,[§] N. Tognalli,[∥] M. dos Santos Afonso,[⊥] and M. L. Martiarena*[,‡]

[†]Instituto Balseiro, Centro Atómico Bariloche (CNEA), Universidad Nacional de Cuyo, Avenida Exequiel Bustillo 9500, 8400 San Carlos de Bariloche, Argentina

[‡]Centro Atómico Bariloche (CNEA), Consejo Nacional de Investigaciones Científicas y Técnicas (CONICET), Avenida Exequiel Bustillo 9500, 8400 San Carlos de Bariloche, Argentina

[§]Instituto de Investigaciones Fisicoquímicas Teóricas y Aplicadas (INIFTA), Consejo Nacional de Investigaciones Científicas y Técnicas (CONICET), 64 y Diagonal 113, 1900 La Plata, Argentina

[∥]Centro de Innovación Tecnológica, Empresarial y Social (CITES), Avenida Belgrano 758, 2322 Sunchales, Argentina

[⊥]Instituto de Química Física de los Materiales, Medio Ambiente y Energía (INQUIMAE) and Departamento de Química Inorgánica, Analítica y Química Física, Facultad de Ciencias Exactas y Naturales, Universidad de Buenos Aires, Ciudad Universitaria, 1428 Buenos Aires, Argentina

Supporting Information

ABSTRACT: Glyphosate [*N*-phosphono-methylglycine (PMG)] is the most used herbicide worldwide, particularly since the development of transgenic glyphosate-resistant (GR) crops. Aminomethylphosphonic acid (AMPA) is the main glyphosate metabolite, and it may be responsible for GR crop damage upon PMG application. PMG degradation into AMPA has hitherto been reckoned mainly as a biological process, produced by soil microorganisms (bacteria and fungi) and plants. In this work, we use density functional calculations to identify the vibrational bands of PMG and AMPA in surface-enhanced Raman spectroscopy (SERS) and attenuated total reflectance Fourier transform infrared (ATR−FTIR) spectra experiments. SERS shows the presence of AMPA after glyphosate is deposited from aqueous solution on different metallic surfaces. AMPA is also detected in ATR−FTIR experiments when PMG interacts with metallic ions in aqueous solution. These results reveal an abiotic degradation process of glyphosate into AMPA, where metals play a crucial role.

KEYWORDS: *glyphosate, AMPA, herbicides, abiotic degradation*

INTRODUCTION

Phosphonates are anthropogenic molecules used in numerous applications as chelating agents and scale inhibitors. They interact strongly with surfaces, resulting in adsorption, dissolution of minerals, remobilization of metals, precipitation of phosphonates, and inhibition of precipitation of minerals.[1] All of these processes, including photo- and biodegradation of phosphonates, are modified by the presence of metals because of the formation of soluble and non-soluble complexes.[2]

Glyphosate [*N*-phosphono-methylglycine (PMG)] is the most used phosphonate because of its systemic and broad spectrum herbicide activity.[3,4] Despite a large body of data from research[1−26] and regulatory testing,[5] assessing the extent of glyphosate degradation under field conditions[4] remains a challenging task. PMG interacts strongly with soil components by forming stable complexes with metal ions,[7] and it is thus considered an immobile compound, which remains strongly adsorbed in soil.[8,9] However, both glyphosate and one of its principal metabolites, aminomethylphosphonic acid (AMPA),[9,10] have frequently been detected in surface waters and even groundwaters.[3]

PMG has been reported to be metabolized by soil microbes (bacteria and fungi)[4] and plants.[10−12] In both cases, the process involves either the oxidative cleavage of the C−N bond to yield AMPA or the breaking of the C−P bond by a C−P lyase to generate sarcosine.[11,12] Abiotic oxidative degradations of both glyphosate and AMPA to sarcosine induced by manganese oxide have been demonstrated by Barrett and McBride.[13]

The degradation of PMG into AMPA is of particular interest. This is because (i) AMPA is the main degradation product of glyphosate,[12,14,15] (ii) AMPA is toxic to some plant species, including GR crops,[11,12,14,16] and (iii) recent results indicate that injury to GR crops after application of glyphosate may be caused by AMPA formed from glyphosate degradation,[11,14] with the extent of this damage strongly depending upon AMPA levels.[16]

Despite that PMG degradation into AMPA has hitherto only been reported to take place by biotic pathways,[3,4] the strong interaction of PMG with metals could trigger its degradation into AMPA as well. It is noteworthy that PMG is exposed not only to soil metallic ions[1,13,15] but also to metals in storage bins[27] as well as metallic nozzles and mineralized water when spraying.

Received: June 23, 2014
Revised: September 12, 2014
Accepted: September 16, 2014
Published: September 16, 2014

In this work, we have carried out two sets of experiments involving PMG interaction with metals: (i) surface-enhanced Raman spectroscopy (SERS) experiments after PMG was deposited from an aqueous solution on different metallic surfaces and (ii) attenuated total reflectance Fourier transform infrared (ATR−FTIR) spectra experiments of PMG interacting with metallic ions in aqueous solution. We have used density functional theory (DFT) calculations to identify the vibrational bands, looking for fingerprints of the AMPA and PMG presence. Both experiments show evidence of an abiotic pathway of PMG degradation into AMPA.

MATERIALS AND METHODS

Raman Experiments. SERS experiments were made *ex situ* using a Jobin-Yvon T64000 triple spectrometer operating in subtractive mode and equipped with a liquid-N_2-cooled charge-coupled device. The excitation was performed using the 647.1 nm line of an Ar−Kr laser. Typical acquisitions employed three integrations of 60 s using laser powers of 20−50 mW, concentrated on a 7 mm long and around 100 mm wide line focus. This was chosen to reduce the photon-induced degradation of the samples. Product formation because of reactions occurring at these excitation wavelengths were further ruled out by checking that the spectra remained constant in time.

Glyphosate and AMPA were purchased from Sigma-Aldrich (analytical standard quality). All other supplies used were of the best analytical grade commercially available.

SERS experiments were performed on sphere segment void (SSV) arrays, fabricated via an hexagonal close packed self-assembly of 600 nm radius polystyrene spheres, followed by an electrochemical Au deposition, as originally described by Bartlett and co-workers.[28,29]

Structured copper surfaces were prepared by underpotential deposition (UPD) on SSV gold arrays from a 5×10^{-4} M $CuSO_4$ + 1 M H_2SO_4 aqueous solution in a conventional electrochemical cell. A voltammetry sweep from −0.6 to 0 V at 0.25 V s^{-1} was performed with a Pt large area foil as the counter electrode and a Cu wire as the pseudo-reference electrode.

Ag nanoparticles (NPs) were deposited to further increase the Raman signal.[6,30,31] These nanoparticles (spheric, 20 nm mean size) were synthesized according to the Turkevich method.[32] Briefly, 100 mL of 1 mM $AgNO_3$ aqueous solution was stirred and heated until 90 °C and then reduced with 20 mg of sodium citrate. After the color change to yellow, the solution was cooled while stirring until room temperature. Always a fresh stash of Ag NPs was used for each experiment.

PMG and AMPA adsorption on SSV substrates was made following two different methods. (I) Drop casting: a 10 μL drop of 1 mg/mL PMG or AMPA aqueous solution with Milli-Q water (18.0 MΩ) was deposited on the SSV surface and dried with N_2 flux; immediately, the sample was dipped in a Ag nanoparticle solution overnight and then rinsed with Milli-Q water and dried with N_2 flux. (II) Dipping: SSV substrate was dipped in 1 mg/mL PMG aqueous solution overnight and then carefully rinsed with Milli-Q water and dried with N_2 flux; finally, 10 μL of Ag nanoparticles were drop-casted on top and dried with N_2 flux.

ATR−FTIR Experiments. The ATR−FTIR experiments were performed in the 500−4000 cm^{-1} region in a Nicolet 8700 FTIR spectrometer (128 scans, resolution of 4 cm^{-1}) equipped with a DTGS detector and a Smart Orbit ATR accessory with a diamond crystal unit with a single reflection. A baseline correction was made for instrumental instabilities, and the background was subtracted. Data were evaluated using OMNIC, version 7.3, Thermo Electron Corporation software.

All chemical reagents were analytical-grade and used without any further purification. Water was purified in a Milli-Q system from Millipore, Inc. Glyphosate was provided by Sigma Co. Copper chloride dehydrated ($CuCl_2 \cdot 2H_2O$) and AMPA (99% pure) were from Aldrich Chemical.

Stock solutions of 1000 mg L^{-1} of each reagent (Cu^{II}, AMPA, and PMG) were prepared. The stock solution of Cu^{II} was prepared by dissolving $CuCl_2 \cdot 2H_2O$ in Milli-Q water. The reactant molar ratios of 2.7:1 Cu^{II}/PMG and 2.6:1 Cu^{II}/AMPA were obtained by adding the required aliquots of Cu^{II} and PMG (or AMPA) stock solutions into a flask, reaching the final volume by the addition of the required volume of Milli-Q water.

The colorless solution of PMG (or AMPA) changed to light blue as soon as the light green solution of $CuCl_2$ was added. The complex solution was frozen and freeze-dried, and a bright green solid was obtained.

DFT Calculations. The DFT calculations were carried out within the slab-supercell approach by means of the Vienna *ab initio* simulation program (VASP).[33−35] The electron−ion interactions were described through the projector-augmented plane-wave (PAW) Perdew−Burke−Ernzerhof (PBE) pseudo-potentials. Exchange and correlation (XC) was described within the van der Waals density functional with optB86b as the exchange functional. We used an energy cutoff of 450 eV, and the Brillouin zone integration was performed within the Methfessel−Paxton technique,[36] with an electron smearing of 0.1 eV. The energies and forces were converged to 10^{-4} eV and 10^{-1} eV/nm. The Cu(111) and Cu(100) surfaces were represented by a 4×4 unit cell with five-layer slabs. AMPA was adsorbed only on one side of the slab, and during full geometry optimizations, we allowed for relaxation of the three topmost layer metal atoms and all of the atoms of the molecule.

RESULTS AND DISCUSSION

We started by characterizing the vibration spectra of PMG[17] and AMPA[18] crystals using DFT calculations. Table 1 shows the theoretical frequencies for PMG and AMPA and the vibration mode identification. The crystals have non-equivalent molecules within the unit cell; consequently, the frequencies in Table 1 correspond to averages over sets of modes in similar vibration states.[37]

From the analysis of the DFT results, we identify the mode at 717 cm^{-1} for AMPA and 761 cm^{-1} for PMG (highlighted in blue in Table 1) as a P−C stretching vibration. This mode is separated from neighboring modes by more than 90 cm^{-1}, with the only exception of a mode appearing at 783 cm^{-1} in the PMG crystal, which corresponds to a complex vibration [ν(PC) + $\rho(CH_2)$ + $\rho(NH_2)$ + ν(CCOO)]. This feature together with the fact that the AMPA P−C and PMG P−C are separated enough from each other makes these modes easily resolvable in vibrational spectra, therefore providing respective fingerprints for the AMPA and PMG presence.

To study the effect of the molecule surface adsorption on the vibrational spectra, we performed DFT calculations for AMPA on Cu(111) and Cu(100) surfaces (see Tables S2 and S3 of the Supporting Information). The calculated P−C mode frequencies shift down, relative to the crystal, 15 and 7 cm^{-1} for Cu(111) and Cu(100) surfaces, respectively.

The Raman spectra obtained for the AMPA and PMG crystals are shown in panels A and B of Figure 1, respectively. Fits of the P−C peaks are shown in blue for PMG and green for AMPA.

We show in Figure 1C the SERS spectrum of PMG deposited from aqueous solutions on Cu_UPD/Au with Ag nanoparticles, using the drop-casting method. It presents a peak at the frequency previously assigned to the P−C mode of the PMG crystal, but unexpectedly, a second peak is also observed. This second peak is in a region free of PMG vibrations and at the frequency of the AMPA P−C mode, indicating the presence of AMPA in this sample. To the best of our knowledge, this

Table 1. DFT-Calculated Frequencies (cm^{-1}) and Vibration Modes for PMG and AMPA Crystals[a]

PMG crystal	AMPA crystal	Vibration modes
	460	δ(HO-P=O)/δ(O=P=O)
473		δ(PO3)+δ(NCCO)
495		δ(HO-P=O)+ρ(PCN)+ δ(NCC)+δ(OH-C=O)+ ρ(CH2)*
520		δ(HO-P=O)+δ(CNC)+ δ(OH-C=O)+ρ(CH2)*
	529	δ(P-C-N)+ω(HO-P=O)
541		δ(HO-P=O)+ δ(PCN)+δ(C=C-OH)
	558	τ(NH3)
559		δρ(PO3)+skel(NCCO2)
629		ν(PC)+δ(NCC)+δ(COO)
	717	ν(PC)
761		ν(PC)
783		ν(PC)+ρ(CH2)+ρ(NH2)+ν(CCOO)
	819	ρ(CH2)+ν(P-OH)
851		ν(CC)
906		CNCC skeleton
	908	ν(HO-P)
948		νs(PO3)+ν(PC)
978		νs(PO3)+τ(CH2)+ ρ(NH2)+skel(CNCC)
	983	ν(OP)
	1007	ν(CN)
999		CNCC skeleton
	1032	ν(PO3)
1039		ν(CN)/CNCC skel+ νa(HO-P=O)/νa(POO)
1059		CNC skeleton
	1078	δ(HNC)+νa(PO2)/ν(PO)
1085		νa(PO3)+ν(NC)
	1107	νa(O=P=O)+δ(HCNH)
1123		νa(P-OH)
	1131	ρ(NH3)
1184		(CH2+NH2+CH2*)/HCNCH+ν(COH)
	1166	ν(P=O)
1226		(CH2+NH2+CH2*)+ν(CN)+ν(COH)
1242		ν(P-OH)+τ(CH2)+ ν(COH) +δ(CNC)
1280		ν(PC)+ν(POH)+ω(CH2)
1303		ω(CH2)+ωτ(CH2)*+ δ(COH)+ν(PC)
	1311	δ(HOP)+ν(PC)+δ(HCNH)
1327		ωτ(CH2)*+δ(COH)+ δ(CNC)/ν(POH)+...
	1339	δ(HCNH)+δ(PCN)
1406		δ(CH2)+ν(CCOH)
1431		δ(CH2)+δ(POH)
	1432	δ(CH2)
1452		ν(CC)+δ(CNH)/τ(NH2)
1485		ω(NH2)+δ(POH)
	1534	δ(NH3)
1567	1628	δ(NH2)
	1653	δ(NH2)
1705		ν(CO)

[a]Mode notation: δ for bending, ν for stretching (ν_a and ν_s for asymmetric and symmetric stretching), ω for wagging, ρ for rocking, τ for twisting, and "skel" for skeleton. In PMG, CH_2* refers to the methyl farthest away from the phosphonate group. For further details, see the captions of Tables S2–S3 of the Supporting Information.

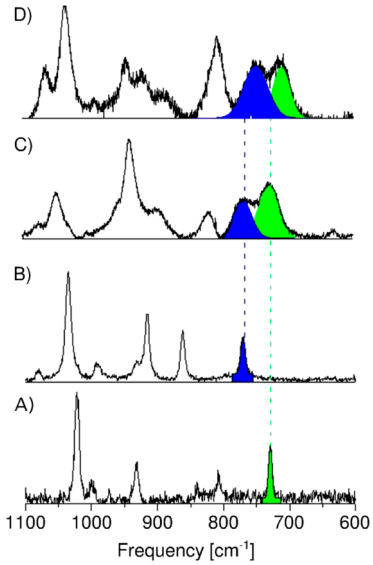

Figure 1. SERS spectra for (A) AMPA crystals, (B) PMG crystals, (C) PMG deposited on Cu_UPD/Au with Ag NPs using the drop-casting method, and (D) PMG deposited on Cu_UPD/Au with Ag NPs using the dipping method. The shadowed areas correspond to the P–C mode region for AMPA (green) and PMG (blue).

result provides the first evidence of an abiotic path for PMG degradation into AMPA.

Figure 1D shows the SERS spectrum of a sample prepared with the dipping method. It is noteworthy that, in this preparation, the samples are rinsed before the addition of Ag NPs, and thus, most of the molecules that are not adsorbed on the surface are removed from it.

The P–C peaks of AMPA and PMG are also present in Figure 1D, even though they are shifted to lower frequencies (shifts of 20 cm^{-1} for AMPA and 22 cm^{-1} for PMG). Based on the DFT results for AMPA/Cu, these experimentally observed shifts to lower frequencies indicate that both AMPA and PMG are predominantly adsorbed on the Cu surface.

From the analysis of Figure 1, we conclude that (i) for both sample preparation methods, an abiotic degradation process of PMG into AMPA has taken place, (ii) when the drop-casting method is used, the P–C mode of PMG and AMPA is not shifted relative to the PMG or AMPA crystal mode, indicating that most of the molecules are not bonded to the Cu surface, and (iii) in samples prepared with the dipping method, the resulting PMG and AMPA are mainly adsorbed on the surface.

An estimation of the percentage of PMG degraded into AMPA can be obtained by means of a fitting procedure of the P–C mode frequency region of panels C and D of Figure 1. The approximate amount of degradation is 56% in drop-casted samples and 50% in dipped samples. For a detailed description, see Figure S1 and Table S1 of the Supporting Information.

From further analysis, some additional information regarding the adsorbed molecule configuration can be extracted. By means of DFT calculations for crystals, the most intense peak in Figure 1C is identified with the stretching P–O mode (931 cm^{-1}) of both PMG and AMPA (see Table 1). In Figure 1D, this peak decreases, implying that the adsorbed molecules interact with the surface via the phosphonic group.

Complementary SERS spectra for drop-casting experiments of PMG deposited on Ag and Au with Ag NPs show that the degradation of PMG into AMPA is not specific to the

dx.doi.org/10.1021/jf502979d | J. Agric. Food Chem. 2014, 62, 9651–9656

interaction of PMG with a Cu surface but also occurs in the presence of other metallic substrates. The spectra obtained (see Figure S2 of the Supporting Information) are very similar to the spectra in Figure 1C; particularly, the P−C peaks of both molecules appear in all of the samples.

The interaction of PMG with metal atoms in solution is known to result in chelate formation.[20,21,24] This raises the question of whether the surface is itself needed for the degradation process or whether the interaction of PMG with isolated metal atoms can also degrade it into AMPA. To elucidate this point, we prepared a mixture of Cu and PMG in aqueous solution (hereafter referred to as PMG + Cu) using a molar ratio of 2.7:1 Cu/PMG and, after sample lyophilization, characterized it by ATR−FTIR experiments. We also measured the ATR−FTIR spectra for AMPA crystals, PMG crystals, and a 2.6:1 Cu/AMPA mixture in aqueous solution (hereafter AMPA + Cu), to use as references. Figure 2 shows the spectra obtained.

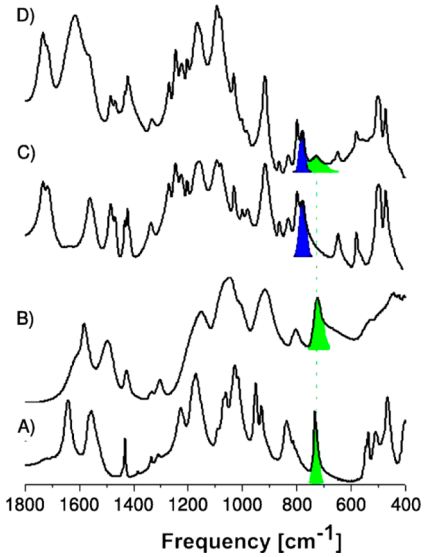

Figure 2. IR spectra of (A) pure AMPA crystals, (B) AMPA + Cu with a molar ratio of 2.6:1 Cu/AMPA, (C) pure PMG crystals, and (D) PMG + Cu with a molar ratio of 2.7:1 Cu/PMG. The shadowed areas correspond to the P−C mode region for AMPA (green) and PMG (blue).

The AMPA P−C peak can be clearly observed in the AMPA (Figure 2A) and AMPA + Cu (Figure 2B) spectra, although slightly shifted to lower frequencies in the latter. Likewise, the PMG P−C peak is present in PMG (Figure 2C) and PMG + Cu (Figure 2D) spectra. For both AMPA and PMG, the respective P−C peaks are distinct and appear at frequencies consistent with the Raman measurements. The PMG spectrum shows a wide gap between the P−C (at 777 cm^{-1}) and the skeleton (at 643 and 577 cm^{-1}) modes. However, in the PMG + Cu spectrum, there is a peak at the frequency of the AMPA P−C mode (729 cm^{-1}), indicating the presence of AMPA molecules and/or AMPA−Cu complexes in the sample.

It must be highlighted that the presence of AMPA in the spectra of PMG + Cu samples is also observed for lower Cu/PMG molar ratios. In fact, the AMPA P−C peak can be clearly identified in samples prepared with a 0.7:1 Cu/PMG molar ratio (see Figure S3 of the Supporting Information).

We find further evidence of PMG into AMPA degradation in the 1600−1700 cm^{-1} region. Our calculations show three vibration modes in the AMPA amino group [$\delta(NH_2)$ at 1648 and 1588 cm^{-1}, and $\delta(NH_3)$ at 1525 cm^{-1}], in agreement with Raman data. Infrared (IR) peaks of AMPA at 1555 and 1641 cm^{-1} correspond to two of these modes. PMG has a single $\delta(NH_2)$ mode at 1567 cm^{-1} (Raman peak at 1568 cm^{-1} and IR peak at 1560 cm^{-1}) and a $\nu(C{=}O)$ mode of the carboxylate group at 1705 cm^{-1}, associated with Raman and IR structures at 1715−1730 cm^{-1}. These two PMG peaks remain in place in the PMG + Cu IR spectrum, but an intense peak in between, at 1616 cm^{-1}, is also visible. In IR spectroscopic studies of PMG + metal complexes,[22,23] this peak is usually assigned to a $\nu_a(COO)$ mode and interpreted as the result of the interactions of the carboxylate group with Cu atoms. However, we observe that the $\nu(C{=}O)$ mode at 1715−1730 cm^{-1} is not affected much by the presence of Cu atoms. We hence conclude that the 1616 cm^{-1} peak is a combination of the PMG $\delta(NH_2)$ mode and the $\delta(NH_2)$ and $\delta(NH_3)$ modes coming from AMPA and AMPA + Cu.

Additionally, some information regarding AMPA and PMG reactivity to Cu atoms can be drawn from Figure 2. In the 900−1200 cm^{-1} region, the main contribution to AMPA spectra comes from the phosphonate group.[24] Consequently, the changes observed when comparing the AMPA and AMPA + Cu spectra in that region are consistent with Cu atoms being bonded to this group. Also, the significant frequency shift in the NH_2−NH_3 region, around 1600 cm^{-1}, signals Cu−N interactions. These features are consistent with our AMPA/Cu adsorption analysis, where we find that the most stable configuration involves both Cu−O and Cu−N bonds.

Tables S2 and S3 of the Supporting Information show the calculated DFT frequencies and the complete band assignment of the SERS and IR spectra.

In conclusion, in this work, we have detected the presence of AMPA in SERS spectra of pure PMG deposited on several metal surfaces and in IR spectra after the PMG interaction with metallic ions in aqueous solution. Only an abiotic degradation process of PMG, where metal atoms play a central role, can explain the presence of AMPA in the experiments reported.

Previous experimental studies of glyphosate−metal complexes have not considered the PMG degradation pathway revealed in this work. Reported IR spectra do not include the frequency region around the P−C modes, or when they do, thus exposing the AMPA P−C peak[25] at approximately 730 cm^{-1}, the presence of AMPA is not taken into account in the analysis.[6,23,25,26] On the basis of the results presented here, it would be enriching to revisit this literature.

Precision in the dose of application of herbicide products is crucial not only to ensure efficient herbicide treatments but also to reduce the unwanted effects on the environment. Then, it is necessary to study the effectiveness of this abiotic degradation process in agriculture conditions.

Consequently, we expect our results will encourage further research to characterize quantitatively this new PMG into AMPA degradation process.

■ ASSOCIATED CONTENT

Supporting Information

Fitting of the SERS spectra in the P−C frequency region (Figure S1), proportion of molecules according to type and configuration relative to the total number of molecules resulting from the fitting of Figure S1 (Table S1), SERS spectra of

glyphosate deposited on different metal surfaces using the drop-casting method (Figure S2), ATR−FTIR spectra of PMG + Cu samples with different molar ratios (Figure S3), and IR, SERS, and DFT frequencies and band assignments for PMG and AMPA (Tables S2 and S3). This material is available free of charge via the Internet at http://pubs.acs.org.

AUTHOR INFORMATION

Corresponding Author

*E-mail: mluz@cab.cnea.gov.ar.

Funding

The authors acknowledge partial support from ANPCyT-Argentina (Projects PICT-2010-1962 and PICT-2008-1260), CONICET (Project PIP 0667), MinCyT-CNRS (LIFAN), Instituto de Nanociencia y Nanotecnología, CNEA, and Universidad Nacional de Cuyo (06/C390 and 06/C383).

Notes

The authors declare no competing financial interest.

ACKNOWLEDGMENTS

The authors thank G. Zampieri for a thorough reading of the manuscript.

REFERENCES

(1) Nowack, B. Environmental chemistry of phosphonates. *Water Res.* **2003**, *37*, 2533−2546.

(2) Vereecken, H. Mobility and leaching of glyphosate: A review. *Pest Manage. Sci.* **2005**, *61*, 1139−1151.

(3) Borggaard, V.; Gimsing, A. L. Fate of glyphosate in soil and the possibility of leaching to ground and surface waters: A review. *Pest Manage. Sci.* **2008**, *64*, 441−456.

(4) Fenner, K.; Canonica, S.; Wackett, L. P.; Elsner, M. Evaluating pesticide degradation in the environment: Blind spots and emerging opportunities. *Science* **2013**, *341*, 752.

(5) Dieter, H. H. The relevance of "non-relevant metabolites" from plant protection products (PPPs) for drinking water: The German view. *Regul. Toxicol. Pharmacol.* **2010**, *56*, 121−125.

(6) Costa, J. C. S.; Ando, R. A.; Sant'Ana, A. C.; Corio, P. Surface-enhanced Raman spectroscopy studies of organophosphorous model molecules and pesticides. *Phys. Chem. Chem. Phys.* **2012**, *14*, 15645−11565.

(7) Khoury, G. A.; Gehris, T. C.; Tribe, L.; Torres Sánchez, R. M.; dos Santos Afonso, M. Glyphosate adsorption on montmorillonite: An experimental and theoretical study of surface complexes. *Appl. Clay Sci.* **2010**, *50*, 167−175.

(8) Laitinen, P.; Rämö, S.; Nikunen, U.; Jauhiainen, L.; Siimes, K.; Turtola, E. Glyphosate and phosphorus leaching and residues in boreal sandy soil. *Plant Soil* **2009**, *323*, 267−283.

(9) Rampazzo, N.; Rampazzo Todorovic, G.; Mentler, A.; Blum, W. E. H. Adsorption of glyphosate and aminomethylphosphonic acid in soils. *Int. Agrophys.* **2013**, *27*, 203−209.

(10) Ndjeri, M.; Pensel, A.; Peulon, S.; Haldys, V.; Desmazieres, B.; Chausse, A. Degradation of glyphosate and AMPA (amino methylphosphonic acid) solutions by thin films of birnessite electrodeposited: A new design of material for remediation processes? *Colloids Surf., A* **2013**, *435*, 154−169.

(11) Reddy, K. N.; Rimando, A. M.; Duke, S. O.; Nandula, V. K. Aminomethylphosphonic acid accumulation in plant species treated with glyphosate. *J. Agric. Food Chem.* **2008**, *56*, 2125−2130.

(12) Franz, J. E.; Mao, M. K.; Sikorski, J. A. Glyphosate: A unique global herbicide. *ACS Monogr.* **1997**, *189*, 653.

(13) Barrett, K. A.; McBride, M. B. Oxidative degradation of glyphosate and aminomethylphosphonate by manganese oxide. *Environ. Sci. Technol.* **2005**, *39*, 9223−9228.

(14) Reddy, K. N.; Rimando, A. M.; Duke, S. O. Amino-methylphosphonic acid, a metabolite of glyphosate, causes injury in glyphosate-treated, glyphosate-resistant. *J. Agric. Food Chem.* **2004**, *52*, 5139−5143.

(15) Duke, S. O. Glyphosate degradation in glyphosate-resistant and -susceptible crops and weeds. *J. Agric. Food Chem.* **2011**, *59*, 5835−5841.

(16) Dinga, W.; Reddya, K. N.; Zablotowicz, R. M.; Bellaloui, N.; Bruns, A. Physiological responses of glyphosate-resistant and glyphosate-sensitive soybean to aminomethylphosphonic acid, a metabolite of glyphosate. *Chemosphere* **2011**, *83*, 593−598.

(17) Knuuttila, P.; Knuuttila, H. The crystal and molecular structure of *N*-(phosphonomethyl)glycine (glyphosate). *Acta Chem. Scand., Ser. B* **1979**, *33*, 623.

(18) Benbrahim, N.; Rahmouni, A.; Ruiz-López, M. F. A theoretical study of medium effects on the structure of the glycine analogue aminomethylphosphonic acid. *Phys. Chem. Chem. Phys.* **2008**, *10*, 5624−5632.

(19) Piccolo, A.; Celano, G. Hydrogen-bonding interactions between the herbicide glyphosate and water-soluble humic substances. *Environ. Toxicol. Chem.* **1994**, *13*, 1737−1741.

(20) Popov, K.; Rönkkömäki, H.; Lajunen, L. H. J. Critical evaluation of stability constants of phosphonic acids. *Pure Appl. Chem.* **2001**, *73*, 1641.

(21) Barja, B. C.; Herszage, J.; dos Santos Afonso, M. Iron(III)−phosphonate complexes. *Polyhedron* **2001**, *20*, 1821−1830.

(22) Subramaniam, V.; Hoggard, P. Metal complex of glyphosate. *J. Agric. Food Chem.* **1988**, *36*, 1326−1329.

(23) Sheals, J.; Persson, P.; Hedman, B. IR and EXAFS spectroscopic studies of glyphosate protonation and copper(II) complexes of glyphosate in aqueous solution. *Inorg. Chem.* **2001**, *40*, 4302−4309.

(24) Barja, B. C.; Dos Santos Afonso, M. Aminomethylphosphonic acid and glyphosate adsorption onto goethite: A comparative study. *Environ. Sci. Technol.* **2005**, *39*, 585−592.

(25) Undabeytia, T.; Morillo, E.; Maqueda, C. FTIR study of glyphosate−copper complexes. *J. Agric. Food Chem.* **2002**, *50*, 1918−1921.

(26) Harris, W. R.; Sammons, R. D.; Grabiak, R. C.; Mehrsheikh, A. Computer simulation of the interactions of glyphosate with metal ions in phloem. *J. Agric. Food Chem.* **2012**, *60*, 6077−6087.

(27) Glyphosate technical fact sheets currently leave the possibility of stored PMG in copper vessels.

(28) Tognalli, N. G.; Fainstein, A.; Calvo, E. J.; Abdelsalam, M.; Bartlett, P. N. Incident wavelength resolved resonant SERS on Au sphere segment void (SSV) arrays. *J. Phys. Chem. C* **2012**, *116* (5), 3414−3420.

(29) Tognalli, N. G.; Cortés, E.; Hernandez-Nieves, A. D.; Carro, P.; Usaj, G.; Balseiro, C.; Vela, M. E.; Salvarezza, R. C.; Fainstein, A. From single to multiple Ag-layer modification of Au nanocavity substrates: A tunable probe of the chemical surface-enhanced Raman scattering mechanism. *ACS Nano* **2011**, *5* (7), 5433−5443.

(30) Fan, M.; Brolo, A. G. Silver nanoparticles self assembly as SERS substrates with near single molecule detection limit. *Phys. Chem. Chem. Phys.* **2009**, *11*, 7381−7389.

(31) Orendorff, C. J.; Gole, A.; Sau, T. K.; Murphy, C. J. Surface-enhanced Raman spectroscopy of self-assembled monolayers: Sandwich architecture and nanoparticle shape dependence. *Anal. Chem.* **2005**, *77*, 3261−3266.

(32) Turkevich, J.; Stevenson, P. C.; Hillier, J. A study of the nucleation and growth processes in the synthesis of colloidal gold. *Discuss. Faraday Soc.* **1951**, *11*, 55−75.

(33) Hafner, R. Ab-initio simulations of materials using VASP: Density-functional theory and beyond. *J. Comput. Chem.* **2008**, *29*, 2044−2078.

(34) Kresse, G.; Hafner, J. Ab initio molecular dynamics for liquid metals. *Phys. Rev. B: Condens. Matter Mater. Phys.* **1993**, *47*, 558−561.

(35) Kresse, G.; Hafner, J. Ab initio molecular-dynamics simulation of the liquid-metal−amorphous-semiconductor transition in germanium. *Phys. Rev. B: Condens. Matter Mater. Phys.* **1994**, *49*, 14251−14269.

(36) Methfessel, M.; Paxton, A. High-precision sampling for Brillouin-zone integration in metals. *Phys. Rev. B: Condens. Matter Mater. Phys.* **1989**, *40*, 3616−3621.

(37) Although in some cases, there were slight differences in either the atoms involved or the vibration mode of a given group. For those cases, the notation mode 1/mode 2 refers to averages over states, some of which include the "mode 1" vibration, while some include the other "mode 2" vibration.